SCIREA Journal of Physics

https://www.scirea.org/journal/Physics

August 10, 2019

Volume 4, Issue 5, October 2019

Effects of Heavy Doping and Impurity Size on Minority-Carrier Transport Parameters in Heavily (Lightly) Doped p^+ (n)-Type Crystalline Silicon at 300 K, Applied to Determine the Performance of $p^+ - n$ Junction Solar Cells

H. Van Cong *, P. Blaise ** and O. Henri-Rousseau

Université de Perpignan Via Domitia, Laboratoire de Mathématiques et Physique (LAMPS), EA 4217, Département de Physique, 52, Avenue Paul Alduy, F-66 860 Perpignan, France

* huynh@univ-perp.fr and huynhvc@outlook.fr

** blaise@univ-perp.fr

Abstract

The effects of heavy doping and acceptor (donor) size on the electron (hole)-minority saturation current density $J_{Eo}(J_{Bo})$, injected respectively into the heavily (lightly) doped crystalline silicon (Si) emitter (base) region of $p^+ - n$ junction, which can be applied to determine the performance of solar cells, being strongly affected by the dark saturation current density: $J_o \equiv J_{Eo} + J_{Bo}$, were investigated. For that, we used an effective Gaussian acceptor-density profile to determine J_{Eo}, and an empirical method of two points to investigate the ideality factor n, short circuit current density J_{sc}, fill factor (FF), and photovoltaic conversion efficiency η, expressed as functions of the open circuit voltage V_{oc}, giving rise to a satisfactory description of our obtained results, being compared also with other existing theoretical-and-experimental ones. In particular, the highest η-value, obtained

in the present paper is equal to: $\eta(\text{present}) = 27.56\%$, given in the condition of completely opaque and heavily doped (Tl-Si) emitter-and-lightly doped (S-Si) base regions, with the intrinsic band gap, $E_{gi}(r_{Tl}) = 1.34$ eV, where r_{Tl} is the Tl-atom radius, while in our previous paper we got: $\eta(\text{previous}) = 31.55\%$, obtained in the condition of completely opaque and heavily doped (S-Si) emitter-and-lightly doped (Tl-Si) base regions, with $E_{gi}(r_S) = 1.70$ eV $> E_{gi}(r_{Tl}) = 1.34$ eV, where r_S is the S-atom radius. That is due to the impurity-size effect, because of $r_S > r_{Tl}$. Those results can be compared with a well-known highest η-value, obtained by Richter et al. (R), $\eta(R) = 29.43\%$, as: $\eta(\text{present}) = 27.56\% < \eta(R) = 29.43\% < \eta(\text{previous}) = 31.55\%$.

Keywords: donor (acceptor)-size effect; heavily doped emitter region; ideality factor; open circuit voltage; photovoltaic conversion efficiency

1. Introduction

In our recent paper [1], which will be henceforth be referred to as I, we studied the effects of heavy doping and impurity size on minority-carrier transport parameters in heavily (lightly) doped n(p)-type crystalline silicon at 300 K, respectively, being applied to determine the performance of $n^+ - p$ junction solar cells. Those effects of heavy doping and donor (acceptor) size on the hole (electron)-minority saturation current density $J_{Eo}(J_{Bo})$, injected respectively into the heavily (lightly) doped crystalline silicon (Si) emitter (base) region of $n^+ - p$ junction, which can be applied to determine the performance of solar cells, being strongly affected by the dark saturation current density: $J_o \equiv J_{Eo} + J_{Bo}$, were investigated. For that, we used an effective Gaussian donor-density profile to determine J_{Eo}, and an empirical method of two points to investigate the ideality factor n, short circuit current density J_{sc}, fill factor (FF), and photovoltaic conversion efficiency η, expressed as functions of the open circuit voltage V_{oc}, giving rise to a satisfactory description of our obtained results, being compared also with other existing theoretical-and-experimental ones. In particular, in I, the highest η-value, obtained in the condition of completely opaque and heavily doped (S-Si) emitter-and-lightly doped (Tl-Si) base regions, was found to be equal to 31.55%.

Then, in the present paper [1-46], we will investigate the effects of heavy doping and impurity size on minority-carrier transport parameters in heavily (lightly) doped p(n)-type crystalline

silicon at 300 K, respectively, being applied to determine the performance of $p^+ - n$ junction solar cells, by using a same treatment method as that given in I.

In Section 2, we study the effects of impurity size [or compression (dilatation)], temperature and heavy doping, affecting all the energy-band-structure parameters such as: the intrinsic band gap E_{gi}, intrinsic carrier concentration n_i, band gap narrowing ΔE_g, Fermi energy E_F, apparent band gap narrowing ΔE_{ga}, and effective intrinsic carrier concentration n_{ie}. In Section 3, using Equations (16, 17), an accurate expression for the optical band gap (OBG), E_{g1}, is investigated, being found to be accurate within 1.88% and 1.46%, respectively, as showed in Table 3. Some useful minority-carrier transport parameters such as: the minority-electron mobility and diffusion length, μ_e and L_e, given in the heavily doped p-type emitter region, and the minority-hole mobility and lifetime, μ_h and τ_h, and the minority-hole saturation current density J_{Bo}, being given in the lightly doped n-type base region, are also presented in Section 4. Then, in Section 5, an accurate expression for the minority-electron saturation current density, J_{Eo}, injected into the heavily doped p-type emitter region of $p^+ - n$ junction silicon solar cells at 300 K is established in Eq. (35) or its approximate form given in Eq. (40). Further, the total saturation current density: $J_o = J_{Eo} + J_{Bo}$, where J_{Bo}, determined in Equation (17), is the minority-hole saturation current density, J_{Bo}, injected into the lightly doped n-type base region of $p^+ - n$ junction silicon solar cells, can be used to investigate the photovoltaic conversion effect, as presented in Section 6. Finally, some concluding remarks are discussed and given in Section 7.

2. Energy-Band-Structure Parameters in Acceptor (Donor)-Si Systems

Here, we study the effects of acceptor (donor) [a(d)]-size, temperature, and heavy doping on the energy-band-structure parameters of a(d)-Si systems, as follows.

2.1. Effect of d(a)-Size

In a(d)-Si systems at T=0 K, since the a(d)-radius $r_{a(d)}$, in tetrahedral covalent bonds is usually either larger or smaller than the Si atom-radius r_o, assuming that in the B(P)-Si system $r_{B(P)} = r_o = 0.117$ nm, with $1\,\text{nm} = 10^{-9}\text{m}$, a local mechanical strain (or deformation potential energy) is induced, according to a compression (dilation) for $r_{a(d)} > r_o$ ($r_{a(d)} < r_o$), respectively, due to the a(d)-size effect. Then, in the Appendix A of our recent paper [43], basing on an effective Bohr model, such a compression (dilatation) occurring in

various a(d)-Si systems was investigated, suggesting that the effective dielectric constant, $\varepsilon(r_{a(d)})$, decreases with increasing $r_{a(d)}$. This $r_{a(d)}$-effect thus affects the changes in all the energy-band-structure parameters, expressed in terms of $\varepsilon(r_{a(d)})$, noting that in the B(P)-Si system $\varepsilon(r_{B(P)}), = 11.4$. In particular, the changes in the unperturbed intrinsic band gap, $E_{go}(r_{B(P)}) = 1.17$ eV , and effective a(d)-ionization energy in absolute values $E_{ao(do)}(r_{B(P)}) = 33.58$ meV, are obtained in an effective Bohr model, as [43]:

$$E_{go}(r_{a(d)}) - E_{go}(r_{B(P)}) = E_{ao(do)}(r_{a(d)}) - E_{ao(do)}(r_{B(P)}) = E_{ao(do)}(r_{B(P)}) \times \left[\left(\frac{\varepsilon(r_{B(P)})}{\varepsilon(r_{a(d)})}\right)^2 - 1\right] \quad (1)$$

Therefore, with increasing $r_{a(d)}$, the effective dielectric constant $\varepsilon(r_{a(d)})$ decreases, implying that $E_{go}(r_{a(d)})$ increase. Those changes, which were investigated in our previous paper [43], are now reported in the following Table 1, in which the data of the critical d(a)-density $N_{cn(cp)}(r_{d(a)})$ are also reported. This critical density marks the metal-to-insulator transition from the localized side (all the impurities are electrical neutral), $N(N_a) \leq N_{cn(cp)}(r_{d(a)})$, to the extended side, $N(N_a) \geq N_{cn(cp)}(r_{d(a)})$, assuming that all the impurities are ionized even at 0 K. However, at $T = 300$ K, for example, all the impurities are thus ionized and the physical conditions, defined by: $N(N_a) > N_{cn(cp)}(r_{d(a)})$ and $N(N_a) < N_{cn(cp)}(r_{d(a)})$, can thus be used to define the n(p)-type heavily and lightly doped Si, respectively.

Table 1. The values of $r_{d(a)}$, $\varepsilon(r_{d(a)})$, and $E_{go}(r_{d(a)})$, and critical impurity density $N_{cn(cp)}(r_{d(a)})$, at T=0 K, obtained in I, are reported here.

Donor	Sb	P	As	Bi	Ti	Te	Se	S
r_d (nm)	0.1131	0.1170	0.1277	0.1292	0.1424	0.1546	0.1621	0.1628
$\varepsilon(r_d)$	12.02	11.40	8.47	7.95	4.71	3.26	2.71	2.67
$E_{go}(r_d)$ (eV)	1.167	1.170	1.197	1.205	1.333	1.547	1.729	1.749
$N_{cn}(r_d)$ (10^{18} cm^{-3})	3	3.52	8.58	10.37	50	150.74	261.24	274.57
At T=300 K, the conditions: $N > N_{cn}(r_d)$ and $N \leq N_{cn}(r_d)$, can thus be used to define the n-type heavily-and-lightly doped Si, respectively.								

Acceptor	B	Al	Ga	In	Tl
r_a (nm)	0.1170	0.1254	0.1263	0.1352	0.1410
$\varepsilon(r_a)$	11.40	8.88	8.49	5.57	4.42
$E_{go}(r_d)$ (eV)	1.170	1.195	1.201	1.292	1.387
$N_{cp}(r_a)$ (10^{18} cm^{-3})	4.06	8.58	9.83	34.73	69.87
At T=300 K, the conditions: $N_a > N_{cp}(r_{a)})$ and $N_a \leq N_{cp}(r_{a)})$, can thus be used to define the p-type heavily-and-lightly doped Si, respectively.					

2.2. Temperature Effect

Being inspired from excellent works by Pässler [34, 35], who used semi-empirical descriptions of T-dependences of band gap of the Si by taking into account the cumulative effect of electron-phonon interaction and thermal lattice expansion mechanisms or all the contributions of individual lattice oscillations [33-35], we proposed in our recent paper [43] a simple accurate expression for the intrinsic band gap in the silicon (Si), due to the T-dependent carrier-lattice interaction-effect, $E_{gi}(T,r_{d(a)})$, as:

$$E_{gi}(T,r_{d(a)}) \simeq E_{go}(r_{d(a)}) - 0.071\ (eV) \times \left\{ \left[1 + \left(\frac{2T}{440.6913\ K} \right)^{2.201} \right]^{\frac{1}{2.201}} - 1 \right\} \qquad (2)$$

where the values of $E_{go}(r_{d(a)})$ due to the d(a)-size effect are given in Table 1 and those of $E_{gi}(T = 300\ K, r_{d(a)})$ tabulated in Table 2. Further, as noted in this Reference 43, in the (P, S)-Si systems, for $0\ K \leq T \leq 3500\ K$, the absolute maximal relative errors of this E_{gi}-result were found to be equal respectively to: 0.22% and 0.15%, calculated using the very accurate complicated results given by Pässler [35]. Then, in the p(n)-type heavily (lightly) doped (HD) silicon at temperature T, the effective mass of the minority (majority) electron can be defined by [32, 33]:

$$\begin{aligned} m_c(T,r_{a(d)}) &= \left[0.9163 \times \left(0.1905 \times \frac{E_{go}(r_{a(d)})}{E_{gi}(T,r_{a(d)})} \right)^2 \right]^{1/3} \times m_o \\ &= 0.3216 \times m_o \times \left(\frac{E_{go}(r_{a(d)})}{E_{gi}(T,r_{a(d)})} \right)^{2/3} \end{aligned} \qquad (3)$$

m_o being the electron rest mass, and the effective mass of the majority (minority) hole yields [32, 33]:

$$\begin{aligned} & m_v(T) \\ & = g_v^{-2/3} \\ & \times \left(\frac{0.443587 + 0.3609528 \times 10^{-2}T + 0.1173515 \times 10^{-3}T^2 + 0.1263218 \times 10^{-5}T^3 .}{1 + 0.4683382 \times 10^{-2}T + 0.2286895 \times 10^{-3}T^2 + 0.7469271 \times 10^{-6}T^3 + 0.} \right. \end{aligned} \qquad (4)$$

which gives $m_v(T = 0\ K) = m_{vo} = 0.3664 \times m_o$. Here, $g_v = 2$ is the effective average number of equivalent valence-band edges. Here, the intrinsic carrier concentration n_i is defined by

$$n_i^2(T,r_{a(d)}) \equiv N_c\left(T,r_{a(d)}\right) \times N_v(T) \times \exp\left(\frac{-E_{gi}\left(T,r_{a(d)}\right)}{k_B T}\right) \quad (5)$$

where, $N_{c(v)}$ is the conduction (valence)-band density of states, given by [32, 33]:

$$N_c\left(T,r_{a(d)}\right) = 2g_c \times \left(\frac{m_c\left(T,r_{a(d)}\right) \times k_B T}{2\pi\hbar^2}\right)^{\frac{3}{2}} \ (cm^{-3}) \quad (6)$$

$$N_v(T) = 2g_v \times \left(\frac{m_v(T) \times k_B T}{2\pi\hbar^2}\right)^{\frac{3}{2}} \ (cm^{-3}). \quad (7)$$

Here, $\hbar = h/2\pi$ is the Dirac's constant, k_B is the Boltzmann constant, and $g_c = 6$ is the effective average number of equivalent conduction-band edges.

Moreover, at T=300 K, using Equations (2, 5), some typical results of E_{gi} and n_i, are calculated as functions of $r_{d(a)}$, and tabulated in following Table 2.

Table 2. Typical values of intrinsic carrier concentration $n_i(T, r_{d(a)}, g_c)$ and intrinsic band gap E_{gi}

Donor	Sb	P	As	Bi	Ti	Te	Se	S
$E_{gi}(300)$ in eV	1.1215	1.1245	1.1515	1.1595	1.2875	1.5015	1.6835	1.7035
$n_i(300K)$ in 10^{10} cm^{-3}	1.13	1.07	6.34×10^{-1}	5.43×10^{-1}	4.56×10^{-2}	7.26×10^{-4}	2.14×10^{-5}	1.46×10^{-5}

Acceptor	B	Al	Ga	In	Tl
$E_{gi}(300)$ in eV	1.1245	1.1495	1.1555	1.2465	1.3415
$n_i(300\ K)$ in 10^{10} cm^{-3}	1.07	6.59×10^{-1}	5.87×10^{-1}	1.01×10^{-1}	1.60×10^{-2}

From those results, one remarks that $n_i(r_{d(a)})$ decreases with increasing $r_{d(a)}$ since $E_{gi}(r_{d(a)})$ increases as observed in this Table 2, being due to the donor (acceptor)-size effect.

2.3. Heavy doping effect

In the HD acceptor-Si system, we can define the effective intrinsic carrier concentration n_{ie}, by

$$n_{ie}^2 \equiv N \times n_o \equiv n_i^2 \times \exp\left[\frac{\Delta E_{ga}}{k_B T}\right] \tag{8}$$

where n_i^2 is determined in Equation (5), N is the total acceptor density, n_o is the density of minority electron at the thermal equilibrium, and the ABGN is defined by:

$$\Delta E_{ga} \equiv \Delta E_g + k_B T \times \ln\left(\frac{N}{N_V}\right) - E_F \tag{9}$$

where N_V is defined in Equation (7), noting that , from Eq. (8), we can also define the "effective acceptor density" by [10]: $N_{Aeff.} \equiv N/\exp\left[\frac{\Delta E_{ga}}{k_B T}\right]$ so that $N_{Deff.} \times n_o \equiv n_i^2$. Further, in Eq. (9), the Fermi energy E_F can also be determined with a precision of the order of 2.11×10^{-4} [40], as that determined in Eq. (A3) of I, in which the reduced donor density u is now simply replaced by the reduced acceptor one: $w = \frac{N}{N_v(T)}$. Furthermore, in Eq. (9), the BGN, ΔE_g, due to the heavy doping effect, can also be determined in Equation (A15) of I, by a similar way, being appropriate to the BGN, obtained now in the HD acceptor-Si systems as:

$$\Delta E_g(N,r_a) \simeq a_1 \times \frac{\varepsilon(r_B)}{\varepsilon(r_a)} \times N_r^{1/3} + a_2 \times \frac{\varepsilon(r_B)}{\varepsilon(r_a)} \times N_r^{\frac{1}{3}} \times (2.503 \times [-E_c(r_s) \times r_s]) + a_3 \times \left[\frac{\varepsilon(r_B)}{\varepsilon(r_a)}\right]^{5/4} \times N_r^{1/4} \times \sqrt{\frac{m_c(T,r_a)}{m_v(T)}} + a_4 \times \sqrt{\frac{\varepsilon(r_B)}{\varepsilon(r_a)}} \times N_r^{1/2} \times 2 + a_5 \times \left[\frac{\varepsilon(r_B)}{\varepsilon(r_a)}\right]^{\frac{3}{2}} \times N_r^{\frac{1}{6}}, \tag{10}$$

where $N_r = \frac{N}{9.999} \times 10^{17}\ cm^{-3}$, $a_1 = 3.15 \times 10^{-3}, a_2 = 5.41 \times 10^{-4}, a_3 = 2.32 \times 10^{-3}, a_4 = 4.195 \times 10^{-3}, a_5 = 9.8 \times 10^{-5}$, and $E_c(r_s)$ is the shift in majority valence-band edge, determined in Eq. (A7) of I, as a function of the effective Wigner-Seitz r_s, by:

$$r_s(N,r_a) \equiv \left(\frac{3g_v}{4\pi N}\right)^{\frac{1}{3}} \times \frac{1}{a_B(r_a)},\ a_B(r_a) = 5.2917715 \times 10^{-9} \times \frac{\varepsilon(r_a)}{m_v}\ (cm),$$

$a_B(r_a)$ being the effective Bohr radius.

Then, in such the P-Si system at 300K, being inspired by the term: $k_BT \times \ln\left(\frac{N}{N_C}\right)$ given in Eq. (9), and also by the last term given in Eq. (10), we propose an empirical form (EF) of the ABGN, as:

$$\Delta E_{ga(EF)} \equiv 9.987 \times 10^{-3} \times \ln\left(\frac{N}{10^{17}\ cm^{-3}}\right) + 1.039 \times 10^{-4} \times N_r^{\frac{1}{6}} \quad . \quad (11)$$

It should be noted that the empirical forms given in Equations (10, 11) have been chosen such that the obtained numerical results of optical band gap (OBG) are accurate as seen in next Table 3.

Now, in d-Si systems at 300 K, our numerical ABGN (ΔE_{ga})-results are calculated as functions of N, using Equations (9, 11), and plotted in the following Fig. 1.

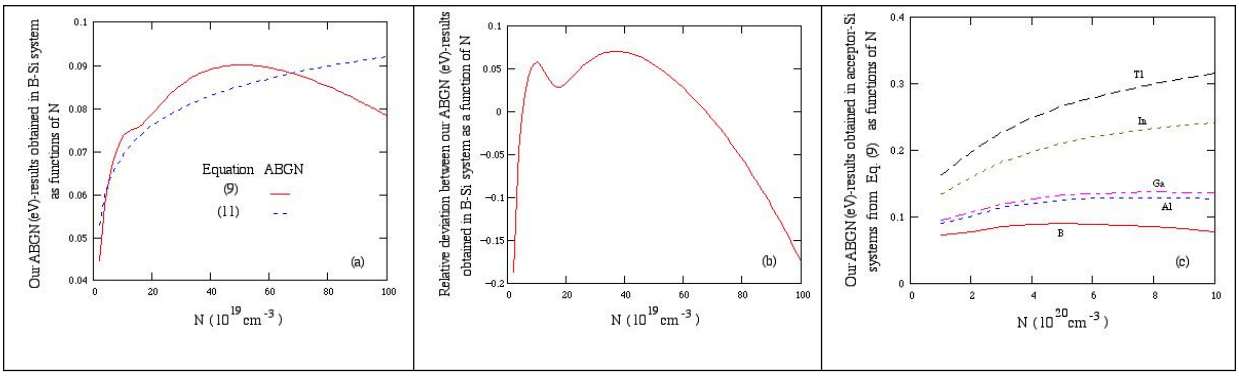

Fig. 1. (a) Comparison of ABGN (ΔE_{ga})-results given in the P-Si system, (b) relative ABGN-deviations given in the P-Si system, and (c) our ABGN-results given in heavily doped acceptor-Si systems, obtained using Eq. (9).

Here, one observes that:

(i) the absolute maximal relative deviation yields about 27.5%, and

(ii) in Fig. 1(c), for a given acceptor (Al, Ga, In, Tl)-Si system, due to the heavy doping effect, or ABGN-result increases with increasing N, and for a given N, due to the donor-size effect, ours increase (↑) with increasing r_a.

3. Conjunction between Electrical-and-Optical Phenomena

First of all, we define the optical band gap (OBG) by [26]:

$$E_{g1(O)}(N,T,r_a) \equiv E_{gi}(T,r_a) - \Delta E_g\,(N, r_a) + E_F(N,r_a), \tag{12}$$

suggesting that the optical phenomenon is represented by $E_{g1(O)}$.

Furthermore, it is possible to establish a conjunction between the electrical (E) and optical (O) phenomena, obtained from Equations (9, 12), by:

$$E_{g1(E)}(N,T,r_a) \equiv E_{gi}(T,r_a) - \Delta E_{ga}\,(N, r_a) + k_B T \times \ln\left(\frac{N}{N_V(T)}\right)$$

which can be rewritten, for example, replacing ΔE_{ga} by $\Delta E_{ga(EF)}$ determined in Eq. (11), as:

$$E_{g1(E)}(N,T,r_a) \equiv E_{gi}(T,r_a) - \Delta E_{ga(EF)} + k_B T \times \ln\left(\frac{N}{N_V(T)}\right). \tag{13}$$

Now, in the P-Si system, our numerical $E_{g1(O,E)}$-results, calculated using Equations (12, 13) for at T=300 K, are tabulated in following Table 3, in which our numerical results of $E_{g1(O)}$ and $E_{g1(E)}$ are accurate within 1.88% and 1.46%, respectively, confirming the accuracy of our empirical forms chosen in Equations (10, 11).

Table 3. Our numerical results of optical band gap, $E_{g1(O,E)}$, expressed as functions of N, and their relative deviations, calculated by: RD(%)=1-(our $E_{g1(O,E)}$-results/ E_{g1}-data), where the E_{g1}-data are given in Ref. 45.

N (10^{18} cm^{-3})	6.5	11	15	26	60	170	400
E_{g1}(eV)-data	1.036	1.044	1.048	1.051	1.062	1.086	1.102
$E_{g1(O)}$(eV)	1.055	1.062	1.066	1.071	1.076	1.092	1.101
RD(%)	-1.87	-1.75	-1.69	-1.88	-1.35	-0.55	0.04
$E_{g1(E)}$(eV)	1.042	1.051	1.055	1.064	1.077	1.094	1.107
RD(%)	-0.60	-0.63	-0.72	-1.26	-1.46	-0.73	-0.50

The underlined |RD|-values are the maximal ones.

4. Minority-Carrier Transport Parameters

Here, in the heavily doped p-type emitter region and the lightly doped n-type base region of $p^+ - n$ junction silicon solar cells, the minority-electron (hole) transport parameters are studied as follows.

4.1. Heavily doped n-type emitter-region parameters

In order to determine the minority-electron saturation-current density J_{Eo}, injected into the heavily doped p-type emitter-region, we need to know an expression for the minority-electron mobility μ_e, being related to the minority-electron diffusion coefficient D_e, by the well-known Einstein relation: $D_e = \frac{k_B T}{e} \times \mu_e$, where e is the positive hole charge. Here, in acceptor-Si systems at 300 K, since the minority-electron mobility depends on N [4], and also $\varepsilon(r_a)$ [12], we can propose:

$$\mu_e(N_a,T,r_a) = \left[92 + \frac{1360 - 92}{1 + \left(\frac{N_a}{1.3 \times 10^{17} cm^{-3}}\right)^{0.91}}\right] \times \left(\frac{\varepsilon(r_a)}{\varepsilon(r_B)}\right)^2 \times \left(\frac{T}{300\ K}\right)^{3/2} (cm^2 V^{-1} s^{-1}) \quad (14)$$

noting that as T = 300 K, and $r_a \equiv r_B$, Eq. (14) is reduced to that investigated by Slotbottom and de Graaff [4], and for a given N and with increasing r_a, μ_e decreases, since $\varepsilon(r_a)$ decreases, as seen in Table 1, in good accordance with that observed by Logan et al. [10]. Further, from Equations (5, 8, 9, 11, 14), we can define the following minority-electron transport parameter F as:

$$F(N,T,r_a) \equiv \frac{n_i^2}{n_o \times D_e} = \frac{N_{Aeff.}}{D_e} \equiv \frac{N}{D_e \times \exp\left[\frac{ABGN}{k_B T}\right]}\ (cm^{-5} \times s),\ N_{Aeff.} \equiv \frac{N}{\exp\left[\frac{ABGN}{k_B T}\right]} \quad (15)$$

where $N_{Deff.}$ is the "effective doping density" [10] and the ABGN is determined in Eq. (9) or Eq. (11).

Furthermore, the minority-electron diffusion length, $L_e(N,T,r_a) = \sqrt{\tau_e \times D_e}$, τ_e being the minority-electron lifetime, can be determined by [23, 26]:

$$L_e^{-2}(N,T,r_a) = [\tau_e \times D_e]^{-1} = (C \times F)^2 = \left(C \times \frac{N_{Aeff.}}{D_e}\right)^2 = \left(C \times \frac{n_i^2}{n_o \times D_e}\right)^2 \quad (16)$$

where the constant $C[=10^{-17}\ (cm^4/s)]$ was chosen in this work. Here, one remarks that τ_e can be computed since D_e (or μ_e) and F are determined respectively in Equations (14, 15).

4.2. Lightly Doped n-type Base-Region Parameters

Here, the minority-hole saturation current density injected into the lightly doped n-type base region, with a donor density equal to N_d, is given by [2, 8]:

$$J_{Bo}(N_d,T,r_d) = \frac{e \times n_i^2(T,r_d) \times \sqrt{\frac{D_h(N_d,T,r_d)}{\tau_h(N_d)}}}{N_d} \quad (17)$$

where $n_i^2(T,r_d)$ is determined in Eq. (5) and $D_h(N_d,T,r_d) \equiv \frac{k_B T}{e} \times \mu_h(N_d,T,r_d)$ is the minority-hole diffusion coefficient, noting that Eq. (17) is valid only for $N_d \leq 10^{16}\ cm^{-3}$.

Here, in the donor-Si system, μ_h is the minority-hole mobility, being determined by [12, 17]:

$$\mu_h(N_d,T,r_d,g_c) = \left[130 + \frac{500-130}{1+\left(\frac{N_d}{8\times10^{17}\ cm^{-3}}\right)^{1.25}}\right] \times \left(\frac{\varepsilon(r_d)}{\varepsilon(r_P)}\right)^2 \times \left(\frac{T}{300\ K}\right)^{3/2}\ (cm^2V^{-1}s^{-1})$$

(18)

being reduced to the result obtained by del Alamo et al. [11, 17], as T=300 K and $r_d = r_P$, and $\tau_h(N_d)$ is the minority-hole lifetime, determined by [26]:

$$\tau_h(N_d)^{-1} = \frac{1}{2.5\times10^{-3}} + 11.76 \times 10^{-13} \times N_d + 2.78 \times 10^{-31} \times N_d^2. \quad (19)$$

Moreover, in Eq. (18), one notes that, for a given N_d and with increasing r_d, μ_h decreases, since $\varepsilon(r_d)$ decreases, as seen in Table 1, in good accordance with that observed by Logan et al. [10].

In the following, we will determine the minority-electron saturation-current density J_{Eo}, injected into the heavily doped p-type emitter-region of the $p^+ - n$ junction solar cells.

5. Minority-Hole Saturation Current Density

Let us first propose in the non-uniformly and heavily doped (NUHD) emitter region of acceptor-Si devices an expression for the effective Gaussian acceptor-density profile or the acceptor (majority-hole) density, being defined in the emitter-region width W, by:

$$\rho(x) = N \times \exp\left\{-\left(\frac{x}{W}\right)^2 \times \ln\left[\frac{N}{N_o(W)}\right]\right\} \equiv N \times \left[\frac{N}{N_o(W)}\right]^{-\left(\frac{x}{W}\right)^2} \quad (20)$$

where $N_o(W) \equiv 2 \times 10^5 \times \exp\left\{-\left(\frac{W}{10^{-7}\,\text{cm}}\right)^{0.5}\right\}\,(\text{cm}^{-3})$, $1\,\mu\text{m} = 10^{-4}\,\text{cm}$, decreases with increasing W, in good agreement with the doping profile measurement on silicon devices, studied by Essa et al. [14]. Moreover, Eq. (20) indicates that:

(i) at the surface emitter: x=0, $\rho(0) = N$, defining the surface acceptor density, and

(ii) at the emitter-base junction: x=W, $\rho(W) = N_o(W)$, which decreases with increasing W, as noted above. Moreover, all the parameters given in Eq. (20) were chosen such that the errors of our obtained J_{Eo}–values are minimized, as seen in next Table 4, and our numerical calculation indicates that, from Equation (20), the highest values of W are found to be: $W \geq 136\,\mu\text{m}$, being equivalent to $W \to \infty$. Then, for example, for $N = 5 \times 10^{20}\,\text{cm}^{-3}$ and with some different values of W, the numerical results of $\rho(x)$ are calculated as a function of the emitter depth x, and then plotted in Fig. 2.

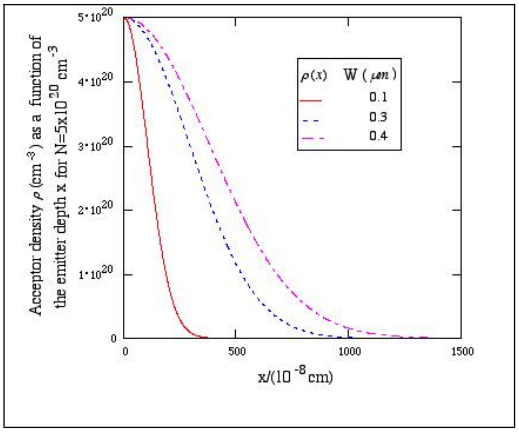

Fig. 2. The numerical results of the effective Gaussian acceptor-density profile $\rho(x)$.

Now, from Eq. (15), for $0 \leq x \leq W$, and using Eq. (20), one has:

$$N_{Aeff.}(x) \equiv \rho(x)/\exp\left[\frac{\Delta E_{ga}(\rho(x))}{k_B T}\right]. \quad (21)$$

Then, under low-level injection, in the absence of external generation, and for the steady-state case, we can define the minority-electron density by:

$$n_o(x) \equiv \frac{n_i^2}{N_{Aeff.}(x)} \quad (22)$$

and a normalized excess minority-electron density [or a relative deviation between $n(x)$ and $n_o(x)$] by [23, 26]:

$$u(x) \equiv \frac{n(x) - n_o(x)}{n_o(x)} \tag{23}$$

which must verify the two following boundary conditions proposed by Shockley as [3]:

$$u(x = 0) \equiv \frac{J_h(x = 0)}{eS \times n_o(x = 0)} \tag{24}$$

$$u(x = W) \simeq \exp\left(\frac{V}{n(V) \times V_T}\right) - 1, \text{ for small } W - \text{values.} \tag{25}$$

Here, $n(V)$ is an ideality factor, $S\ (\frac{cm}{s})$ is the hole surface recombination velocity at the emitter contact, V is the applied voltage, $V_T \equiv (k_B T/e)$ is the thermal voltage, and the minority-electron current density $J_e(x)$, being found to be similar to the Fick's law for diffusion equation, is given by [9, 23]:

$$J_e(x) = \frac{en_i^2}{F(x)} \times \frac{du(x)}{dx} = -\frac{en_i^2 D_e(x)}{N_{Aeff.}(x)} \times \frac{du(x)}{dx} \tag{26}$$

where $F(x)$ is determined in Eq. (19), in which N is replaced by $\rho(x)$, proposed in Equation (20).

Further, the minority-electron continuity equation yields [9, 23]:

$$\frac{dJ_e(x)}{dx} = en_i^2 \times \frac{u(x)}{F(x) \times L_e^2} = en_i^2 \times \frac{u(x)}{N_{Aeff.}(x) \times \tau_e(\rho(x))} = e \times [n(x) - n_0(x)] \times \frac{\tau_e(N)}{\tau_e(\rho(x))} \times \frac{1}{\tau_e(N)}. \tag{27}$$

Then, from these two Equations (26, 27), one obtains the following second-order differential equation as [1, 23]:

$$\frac{d^2u(x)}{dx^2} - \frac{dF(x)}{dx} \times \frac{du(x)}{dx} - \frac{u(x)}{L_e^2(x)} = 0 \tag{28}$$

Using the two boundary conditions (24, 25), one thus gets the general solution of this Equation (28) as [1, 23]:

$$u(x) = [A(W) \times \sinh(P(x)) + B(W) \times \cosh(P(x))] \times \left(\exp\left(\frac{V}{n(V) \times V_T}\right) - 1\right), \tag{29}$$

where $A(W) \equiv \frac{1}{\sinh(P(W)) + I(W) \times \cosh(P(W))}$, $I(W,S) \equiv \frac{B}{A} = \frac{D_e(N_o(W))}{S \times L_e(N_o(W))}$ and $P(x) \equiv \int_0^x C \times F(x)dx$, since $\frac{dP(x)}{dx} \equiv C \times F(x)$. Here, $C = 10^{-17}\ (cm^4/s)$, as that chosen in Eq. (16), and the hyperbolic sine-and-cosine functions are defined by: $\sinh(x) \equiv 0.5 \times [e^x - e^{-x}]$ and $\cosh(x) \equiv 0.5 \times [e^x + e^{-x}]$.

Further, from Eq. (29), as $P(W) \ll 1$ (or for small W) one has: $A \simeq \frac{1}{I}$ or $B \simeq 1$, and one therefore obtains: $u(W) \simeq \left[\exp\left(\frac{V}{n(V)\times V_T}\right) - 1\right]$, which is just the boundary condition given in Eq. (25).

Now, using Equations (26, 29) at T=300 K, one gets:

$$J_e(x, N, r_a, S) = J_{Eo}(x, N, T, r_a, S) \times \left(\exp\left(\frac{V}{n(V) \times V_T}\right) - 1\right) \tag{30}$$

where J_{Eo} is the minority-hole saturation current density, being injected into the heavily doped p-type emitter region, for $0 \le x \le W$, and given by:

$$J_{Eo}(x, N, r_a, S) = en_i^2 C \times [A(W) \times \cosh(P(x)) + B(W) \times \sinh(P(x))] \tag{31}$$

One also remarks that, from Equations (16, 29-31), and after some manipulations, one gets: $u(x = 0) \equiv \frac{J_e(x=0)}{eS \times n_o(x=0)}$, being just the boundary condition given in Eq. (24).

Now, using the P(x)-definition given in Equation (29), one can define the inverse effective minority-electron diffusion length by:

$$\frac{1}{L_{e,eff.}(x = W, N, r_a)} = \frac{1}{W}\int_0^W \frac{dx}{L_e(x)} = \frac{1}{W}\int_0^W C \times F(x)dx \equiv P(x = W, N, r_a)/W \tag{32}$$

where $L_e = (CF)^{-1}$ is defined in Equation (16), in which N is replaced by $\rho(x)$, being determined in Equation (20). Therefore, for a simplicity, Eq. (32) can be rewritten as:

$$P(x = W, N, r_a) \equiv \frac{W}{L_{e,eff.}} = \frac{W}{L_e} \times \frac{L_e}{L_{e,eff.}} \tag{33}$$

Then, from Eq. (29, 31), since $B = A \times I(W,S)$, one obtains:

$$J_{Eo}(x = 0, N, r_a, S) = en_i^2 C \times A = \frac{en_i^2 C}{\sinh(P) + I \times \cosh(P)} \tag{34}$$

$$J_{Eo}(x = W, N, r_a, S) = en_i^2 C \times \frac{\cosh(P) + I \times \sinh(P)}{\sinh(P) + I \times \cosh(P)} \tag{35}$$

Now, from those results (30, 34, 35), one gets:

$$\frac{J_e(x = 0, N, r_a, S)}{J_e(x = W, N, r_a, S)} \equiv \frac{J_{Eo}(x = 0, N, r_a, S)}{J_{Eo}(x = W, N, r_a, S)} = \frac{1}{\cosh(P) + I \times \sinh(P)} \tag{36}$$

Further, using Equations (23, 29, 30) and going back to the minority-electron continuity equation defined in Eq. (27), one gets:

$$\frac{1}{J_{Eo}(x=W)} \times \left[J_{Eo}(x=W) - J_{Eo}(x=0) = \frac{1}{\tau_e(N)} \times Q_{e,\,eff.}(x=W,N)\right] \quad , \tag{37}$$

where $\tau_e(N,r_a)$ is determined in Eq. (16), and $Q_{e,\,eff.}(C/cm^2)$ is the effective excess minority-electron charge density given in the emitter region, defined by [1, 23]:

$$Q_{e,\,eff.}(x=W,N) \equiv \int_0^W e \times [n(x) - n_0(x)] \times \frac{\tau_e(N)}{\tau_e(\rho(x))} dx. \tag{38}$$

Finally, from Equations (36, 37), if defining the effective minority-hole transit time by: $\tau_{t,eff.}(x=W,N,S) \equiv Q_{e,\,eff.}(x=W,N)/J_{Eo}(x=W,N,r_a,S)$, one then obtains the reduced effective minority-electron transit time, as [1, 23]:

$$\frac{\tau_{t,eff.}(x=W,N,r_d,g_c,S)}{\tau_e} = 1 - \frac{J_{Eo}(x=0,N,r_a,S)}{J_{Eo}(x=W,N,r_a,S)} = 1 - \frac{1}{\cosh(P)+I\times\sinh(P)}. \tag{39}$$

Now, from above Equations (34-39), some important results can be obtained and discussed below.

5.1. Very large $S(\geq 10^{50}\ \frac{cm}{s},\ for\ example)$ or $S \to \infty$ and $P \ll 1$ or $W \ll L_{h,eff.}$

Here, various results can be investigated as follows.

(i) From Equations (34-36), since $I(W) = \frac{D_e(N_o(W))}{S\times L_e(N_o(W))} \to 0$ as $S \to \infty$, $\frac{J_{Eo}(x=0,N,r_a,S)}{J_{Eo}(x=W,N,r_a,S)} \simeq \frac{1}{\cosh(P)} \to 1$ since $P \ll 1$, or $J_{Eo}(x=W,N,r_a,S\to\infty) \simeq J_{Eo}(x=0,N,r_a,S\to\infty)$. Therefore, from Eq. (35), one obtains: $\frac{\tau_{t,eff.}(x=W,N,r_d,g_c,S\to\infty)}{\tau_h(N)} \to 0$, suggesting a completely transparent emitter region (CTER).

(ii) Further, from Equations (18-20, 39), since $I \to 0$ and $P \ll 1$, the result (35) is now reduced to:

$$J_{Eo}(x=W,N,r_a,S\to\infty) \simeq \frac{en_i^2C}{P} = \frac{en_i^2}{F\times W}\times\frac{L_{e,eff.}}{L_e} = \frac{en_i^2\times D_e\times\exp\left[\frac{ABGN}{k_BT}\right]}{N\times W}\times\frac{L_{e,eff.}}{L_e} = \frac{en_i^2\times D_e}{N_{Aeff}\times W}\times\frac{L_{e,eff.}}{L_e}, \tag{40}$$

being found to be independent of S and C, since $\frac{L_{h,eff.}}{L_h}$ is independent of S and C, as observed in Equations (16, 32), and noting that the ABGN-expression is determined by Eq. (9) or by Eq. (11).

It should be noted that Cuevas et al. (CFY) [22] used a simplified form as: $J_{Eo(C)} \simeq \frac{en_i^2\times D_e}{N_{Aeff}\times W}$ to explain their experimental results obtained from the samples: 2B1, 2B2, 2B3, 2B4 and 2B5, as those given in Table 1 of this Reference 22, giving the relative deviations in absolute

values equal to: 28.6%, 0%, 66.7%, 220% and 200%, respectively. It means that this simplified $J_{Eo(C)}$ -formula is found to be inaccurate, due to the fact that they neglected an important $(\frac{L_{e,eff.}}{L_e})$-effect, given in this heavily doped emitter region.

Now, in the B-Si system, for $T = 300$ K,$r_a \equiv r_B$, our two numerical J_{Eo}-results are calculated, using Equations (40, 9) and (40, 11), and tabulated in Table 4, in which the CTER -condition, $P \ll 1$ or $\frac{\tau_{t,eff.}}{\tau_e(N)} \ll 1$, is fulfilled, and we also compare them with modeling and measuring J_{Eo}-results investigated by Cuevas et al. (CFY) [22].

Table 4. Our present results of J_{Eo}, expressed as functions of N and W, and the corresponding relative deviations (RDs), calculated, using: RD(%)=1-(Calculated J_{Eo}/ J_{Eo}-data), using the J_{Eo}-data given by Cuevas et al. CFY [22], their calculated results [22], CFY- J_{Eo}, and the corresponding RDs.

N (10^{19} cm^{-3})	2	6	20	60	100
W (μm)	0.19	0.20	0.21	0.23	0.25
$D_{e(CFY)}(cm^2/s)$	2.6	1.8	1.5	1.3	1.3
J_{Eo} − data(A/cm^2)	7×10^{-12}	3×10^{-12}	1.5×10^{-12}	5×10^{-13}	5×10^{-13}
CFY- $J_{Eo}(A/cm^2)$	5×10^{-12}	3×10^{-12}	2.5×10^{-12}	1.6×10^{-12}	1.5×10^{-12}
RD(%)	28.6	0	-66.7	-220	-200
N_o(cm^{-3})	0.2064	0.1443	0.1017	0.052	0.027
$D_e(cm^2/s)$	2.710	2.501	2.420	2.394	2.388
Present J_{Eo}-results are obtained, using Equations (40, 9)					
$\frac{\tau_{t,eff}}{\tau_h(N)} \ll 1$	7.6×10^{-10}	2.5×10^{-9}	9.5×10^{-9}	3.8×10^{-8}	1.5×10^{-7}
Present $J_{Eo}(A/cm^2)$	4.714×10^{-12}	2.596×10^{-12}	1.328×10^{-12}	6.644×10^{-13}	3.391×10^{-13}
RD(%)	32.6	13.5	11.4	-32.9	32.2
Present J_{Eo}-results are obtained, using Equations (40, 11)					
$\frac{\tau_{t,eff}}{\tau_h(N)} \ll 1$	3.4×10^{-10}	1.8×10^{-9}	9.9×10^{-9}	4.7×10^{-8}	1.0×10^{-7}
Present $J_{Eo}(A/cm^2)$	7.065×10^{-12}	3.022×10^{-12}	1.298×10^{-12}	5.967×10^{-13}	4.027×10^{-13}
RD(%)	-0.93	-0.73	13.4	-19.3	19.4

The underlined |RD|-values are the maximal ones, being equal to: 220% for CFY- J_{Eo} [22], and 32.9% and 20.4% for our present J_{Eo} - results, calculated using Equations (40, 9) and (44,11), respectively.

Table 4 indicates that: (1) the RDs between our J_{Eo}–values and measured CFY- J_{Eo} ones are well minimized, confirming that all the parameters given in Eq. (20) have been well chosen, and (2) since for $N \geq 6 \times 10^{20}\ cm^{-3}$, the measured CFY- J_{Eo} values are not regular (for example, they obtained the same results of $D_{e(CFY)}$ and CFY- J_{Eo}. Furthermore, one notes that our ΔE_{ga} -expression given in Eq. (9) has been obtained, taking into account all the physical effects such as: those of acceptor size, heavy doping and Fermi-Dirac statistics, while in Equation (11) our $\Delta E_{ga(EF)}$ -expression is only an empirical ABGN-form. So, we will choose the ABGN-result (9) for all the following numerical calculations.

(iii) Furthermore, in particular, for large S and small P, from Equation (36) one gets:

$$\frac{J_{Eo}(x=0,N,r_a,S)}{J_{Eo}(x=W,N,r_a,S)} = \frac{1}{\cosh(P)+I\times\sinh(P)} \simeq 1 - \frac{D_e(N_o(W))}{S\times L_e(N_o(W))} \times P - \frac{(P)^2}{2}.$$

Then, from Equation (39), using Equations (16, 33) one obtains in the heavily doped case:

$$\begin{aligned}\tau_{t,eff.}(x=W,N,r_a,S) &\simeq \tau_e \times \left\{\frac{D_e(N_o(W))}{S\times L_e(N_o(W))} \times P + \frac{(P)^2}{2}\right\} \\ &\simeq \frac{W}{S} \times \frac{L_e(N_o(W))}{L_{e,eff.}(N_o(W))} + \frac{W^2}{2D_e(N_o(W))} \times \left(\frac{L_e(N_o(W))}{L_{e,eff.}(N_o(W))}\right)^2 \\ &\simeq \frac{W^2}{2D_e(N_o(W))} \times \left(\frac{L_e(N_o(W))}{L_{e,eff.}(N_o(W))}\right)^2, \text{as } S \to \infty\end{aligned} \tag{41}$$

and in the lowly doped case (i.e., $L_{e,eff.} \simeq L_e$):

$$\tau_{t,eff.}(x=W,N,r_a,S) \equiv \tau_t = \frac{W}{S} + \frac{W^2}{2D_e} \simeq \frac{W^2}{2D_e}, \text{ as } S \to \infty \tag{42}$$

being just a familiar expression given for the minority-hole transit time τ_t obtained by Shibib et al. [8].

5.2. Small $S = 10^{-50}$ $(\frac{cm}{s})$ or $S \to 0$, and $P \gg 1$ or $W \gg L_{h,eff.}$

Here, from Eq. (29) and for any N, one has: $I = \frac{D_e(N_o(W))}{S\times L_e(N_o(W))} \to \infty$, since $S \to 0$. Therefore, from Equation (39), one obtains: $\frac{\tau_{t,eff.}(x=W\gg \mathbf{L_{e,eff.}},N,r_a,S\to 0)}{\tau_e} \to 1$, suggesting a completely opaque emitter region (COER).

Then, in the B-Si system at 300 K, our numerical results of $J_{Eo}(x = W, N, r_a, S) \equiv J_{Eo}$ and $\frac{\tau_{t,eff.}(x=W,N,r_a,S)}{\tau_e} \equiv \frac{\tau_{t,eff.}}{\tau_e}$, for simplicity, are computed, using Equations (35, 39), and plotted into Fig. 3 and Fig. 4, respectively, noting that all the above discussions are presented in those Figures (3, 4).

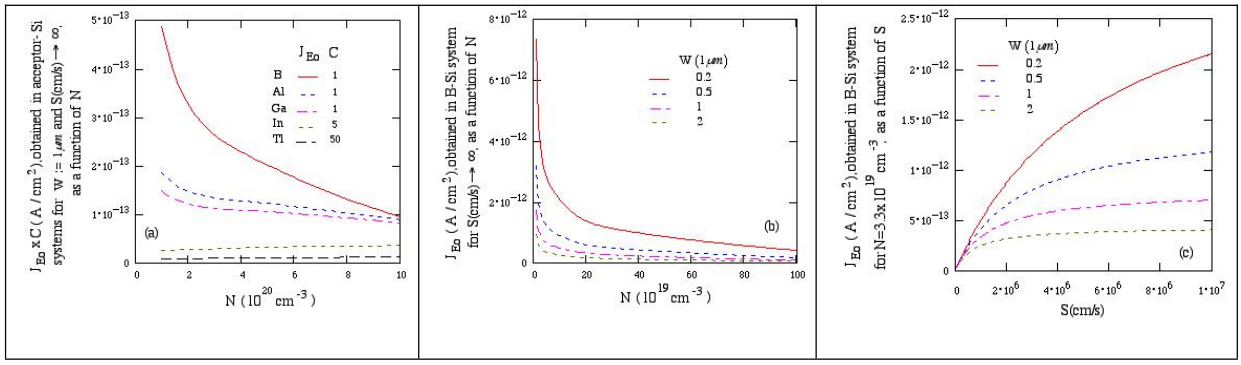

Fig. 3. (a, b) Our J_{Eo}-results obtained as functions of N, (c) our J_{Eo}-ones obtained as functions of S.

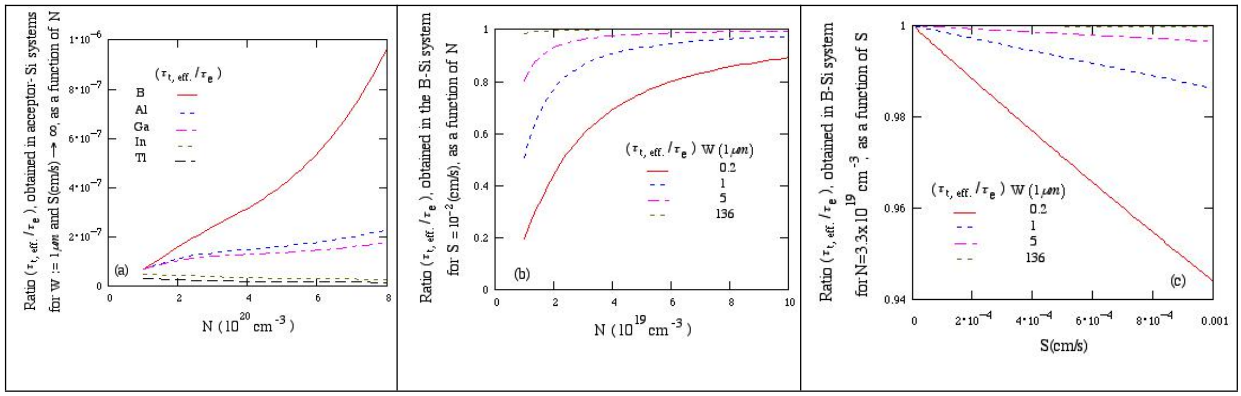

Fig. 4. (a, b) Our $(\tau_{t,\,eff.}/\tau_e)$-results obtained as functions of N, (c) our $\left(\frac{\tau_{t,\,eff.}}{\tau_e}\right)$-ones obtained as functions of S.

Finally, it should be noted that in next Section 6 we must know the numerical results of dark saturation current density, defined by:

$$J_o(x = W, N, r_a, S, N_d, r_d) \equiv J_{Eo}(x = W, N, r_a, S) + J_{Bo}(N_d, r_d) \qquad (43)$$

where J_{Bo} and J_{Eo} are determined respectively in Equations (17, 35). Then, those are tabulated in the following Table 5, in which all the physical conditions are also presented.

Table 5. Our numerical results of $J_o = J_{Eo} + J_{Bo}$, calculated using Eq. (43).

First case: In the heavily doped (HD) B-Si emitter region ($N = 10^{20}\ cm^{-3}$), and in the lightly doped (LD) P-Si base region ($N_d = 10^{16}\ cm^{-3}$) in which $J_{Bo} = 7.26887 \times 10^{-13}\ \left(\frac{A}{cm^2}\right)$.

For $S = 10^{50}\ cm/s$ and $W = 0.206\ nm$, according to the completely transparent emitter region, one has:

$J_{Eo} = 1.71228 \times 10^{-9}\ \left(\frac{A}{cm^2}\right) \gg J_{Bo}$ and $J_o = 1.71301 \times 10^{-9}\ \left(\frac{A}{cm^2}\right) \simeq J_{Eo}$

For $S = 10^{50}\ cm/s$ and $W = 4.4\ nm$, according also to the completely transparent emitter region, one has:

$J_{Eo} = 8.20629 \times 10^{-11}\ \left(\frac{A}{cm^2}\right) \gg J_{Bo}$ and $J_o = 8.27898 \times 10^{-11}\ \left(\frac{A}{cm^2}\right) \simeq J_{Eo}$

For $S = 10^{4}\ cm/s$ and $W = 0.36\ \mu m$, one has:

$J_{Eo} = 1.97026 \times 10^{-15}\ \left(\frac{A}{cm^2}\right) \ll J_{Bo}$ and $J_o = 7.28858 \times 10^{-13}\ \left(\frac{A}{cm^2}\right) \simeq J_{Bo}$

For $S = 10^{-50}\ cm/s$ and $W = 136\ \mu m$, according also to the completely opaque emitter region, one has:

$J_{Eo} = 3.78487 \times 10^{-18}\ \left(\frac{A}{cm^2}\right) \ll J_{Bo}$ and $J_o = 7.26891 \times 10^{-13}\ \left(\frac{A}{cm^2}\right) \simeq J_{Bo}$

Second case: In the completely opaque HD Tl-Si emitter region ($N = 5 \times 10^{20}\ cm^{-3}$, $S = 10^{-50}\ cm/s$ and $W = 136\ \mu m$), where $J_{Eo} = 4.23 \times 10^{-22}\ \left(\frac{A}{cm^2}\right)$, and in the limiting lightly doped d-Si base region, in which $N_d = 10^{16}\ cm^{-3}$.

(r_{Tl}, r_d)	(r_{Tl}, r_{Sb})	(r_{Tl}, r_P)	(r_{Tl}, r_{As})	(r_{Tl}, r_{Bi})	(r_{Tl}, r_{Ti})	(r_{Tl}, r_{Te})	(r_{Tl}, r_{Se})	(r_{Tl}, r_S)
$J_{Bo}\ \left(\frac{A}{cm^2}\right)$	3.505×10^{-14}	3.097×10^{-14}	1.718×10^{-14}	1.547×10^{-14}	7.685×10^{-15}	5.148×10^{-15}	4.257×10^{-15}	4.185×10^{-15}
$J_o\ \left(\frac{A}{cm^2}\right)$	3.505×10^{-14}	3.097×10^{-14}	1.718×10^{-14}	1.547×10^{-14}	7.685×10^{-15}	5.148×10^{-15}	4.257×10^{-15}	4.185×10^{-15}

Thus, $J_o = J_{Bo}$, since $J_{Eo} \simeq 0$.

Third case: In the completely transparent HD a-Si emitter region ($N = 5 \times 10^{20}\ cm^{-3}$, $S = 10^{50}\ cm/s$ and $W = 0.000206\ \mu m$), and in the lightly doped S-Si base region, in which $J_{Bo} = 1.70124 \times 10^{-13}\ \left(\frac{A}{cm^2}\right)$ for $N_d = 10^{16}\ cm^{-3}$.

(r_S, r_a)	(r_S, r_B)	(r_S, r_{Al})	(r_S, r_{Ga})	(r_S, r_{In})	(r_S, r_{Tl})
$J_{Eo}\ \left(\frac{A}{cm^2}\right)$	7.164×10^{-10}	4.345×10^{-10}	3.760×10^{-10}	2.318×10^{-11}	7.935×10^{-13}
$J_o\ \left(\frac{A}{cm^2}\right)$	7.165×10^{-10}	4.347×10^{-10}	3.762×10^{-10}	2.335×10^{-11}	9.636×10^{-13}

Some important remarks are given and discussed below.

(i) In the first case, with decreasing S and increasing W, J_o thus decreases from the CTER to the COER, and one gets in this COER-condition: $J_o \simeq J_{Bo}$.

(ii) In the second case or in the COER-condition, J_{Bo} decreases with increasing r_d, being due to the donor-size effect, and for given r_d one has: $J_o = J_{Bo}$ since $J_{Eo} \simeq 0$.

(iii) In the third case or in the CTER-condition, J_{Eo} decreases with increasing r_a, being due to the acceptor-size effect.

It should be noted that these values of J_o will strongly affect the variations of various photovoltaic conversion parameters of $p^+ - n$ junction silicon solar cells, such as: the ideality factor n, short circuit current density J_{sc}, fill factor FF, and photovoltaic conversion efficiency η, being expressed as functions of the open circuit voltage, V_{oc} [1, 5], as investigated in the following. Our empirical treatment method used here is that of two points [1]. The first point is characterized by [29]:

$$V_{oc1} = 636 \text{ mV}, \; J_{sc1} = 36.9 \, \frac{\text{mA}}{\text{cm}^2}, \tag{44}$$

and the second one by [29]:

$$V_{oc2} = 704 \text{ mV}, J_{sc2} = 41.6 \, \frac{\text{mA}}{\text{cm}^2}. \tag{45}$$

In the following, we will develop our empirical treatment method of two points, used to determine the performance of $p^+ - n$ junction solar cells.

6. Photovoltaic Conversion Effect

The well-known net current density J at T=300 K, expressed as a function of the applied voltage V, flowing through the $p^+ - n$ junction of silicon solar cells, is defined by:

$$J(V) \equiv J_{ph.}(V) - J_o \times \left(e^{\frac{V}{n(V) \times V_T}} - 1 \right), V_T \equiv \frac{k_B T}{e} = 25.8543 \text{ mV} \tag{46}$$

noting that $J(V) = 0$ at $V = V_{oc}$, V_{oc} being an open circuit voltage, at which $J_{ph.}(V = V_{oc}) \equiv J_{sc}(W,N,r_a,S,N_d,r_d,V_{oc})$, where J_{sc} is the short circuit current density. Here, $J_{ph.}$ is the photocurrent density and $J_o(W,N,r_a,S,N_d,r_d) \equiv J_{Eo} + J_{Bo}$ is the "dark saturation current density" or the $p^+ - n$ junction leakage saturation current density in the absence of light, defined in Equation (43). Therefore, the photovoltaic conversion effect occurs, according to:

$$J_{sc}(W,N,r_a,S,N_d,r_d,V_{oc}) \equiv J_o(W,N,r_a,S,N_d,r_d) \times (e^v - 1),\ v(W,N,r_a,S,N_d,r_d,V_{oc}) \equiv \frac{V_{oc}}{n(V) \times V_T} \quad (47)$$

Here, n is the ideality factor, being determined by our empirical treatment method of two points, as:

$$n(W,N,r_a,S,N_d,r_d,V_{oc}) = n_1(W,N,r_a,S,N_d,r_d,V_{oc1},J_{sc1}) + n_2(W,N,r_a,S,N_d,r_d,V_{oc2},J_{sc2}) \times \left(\frac{V_{oc}}{V_{oc1}} - 1\right)^{y_n}, \quad (48)$$

which is valid for any $W,N,r_a,S,N_d,r_d,V_{oc} \geq V_{oc1}$, and increases with increasing V_{oc} for given W,N,r_a,S,N_d and r_d, noting that will be chosen such that the following definition of $n_{1(2)}$ is correct.

Further, the values of V_{oc1},J_{sc1}, V_{oc2} and J_{sc2} are given in Equations (44, 45), and the numerical results of $n_{1(2)}$ can be determined by:

$$n_{1(2)}\left(W,N,r_a,S,N_d,r_d,V_{oc1(2)},J_{sc1(2)}\right) \equiv \frac{V_{oc1(2)}}{V_T} \times \frac{1}{\ln\left(\frac{J_{sc1(2)}}{J_o} + 1\right)} \quad (49)$$

which implies that both $n_{1(2)}$ (or n) and J_o have the same variations for given (W,N,r_a,S,N_d,r_d)-variations, suggesting thus an important remark.

Furthermore, in Eq. (48), for the CTER-conditions such as:

$$W = 0.000206\ \mu m, N = 10^{20}\ cm^{-3}, r_a = r_B, S = 10^{50}\frac{cm}{s}, N_d = 10^{16}\ cm^{-3}, r_d = r_P, \quad (50)$$

one obtains: $n_{1(2)} = 1.45684\ (1.60123)$, according to the value of the exponent y_n, given in Eq. (48), equal to 1.07616.

Then, the values of the fill factor FF, obtained as a function of V_{oc}, can be proposed by:

$$FF(W,N,r_a,S,N_d,r_d,V_{oc}) = \frac{v(W,N,r_a,S,N_d,r_d,V_{oc}) - \ln[v(W,N,r_a,S,N_d,r_d,V_{oc}) + 0.72]}{v(W,N,r_a,S,N_d,r_d,V_{oc}) + y_{FF}} \quad (51)$$

where $y_{FF} = 0.7$ was chosen such that, under the above conditions (50), the values of FF are found to be equal about to 80%, noting that, in the case where both series resistance and shunt resistance have a negligible effect upon cell performance, $y_{FF_{Green}} = 1$, as proposed by Green [5].

Finally, the photovoltaic conversion efficiency η can be defined by:

$$\eta(W,N,r_d,S,N_a,r_a,V_{oc}) \equiv \frac{J_{sc} \times V_{oc} \times FF}{P_{in.}} \quad (52)$$

where J_{sc} and FF are determined respectively in Equations (47, 51), being assumed to be obtained at 1 sun illumination or at AM1.5G spectrum ($P_{in.} = 0.100\ \frac{W}{cm^2}$) [28, 29].

In summary, all above parameters such as: n, J_{sc}, FF and η, defined in above, strongly depend on J_o, determined in Equation (43), which is thus a central result of the present paper.

Now, for given physical conditions such as: W,N,r_a,S,N_d and r_d, and by taking into account all remarks given in Table 5 and also in above Equation (49), our numerical results of n, J_{sc}, FF and η, expressed as functions V_{oc}, are respectively computed, using Equations (48, 47, 51, 52), and reported in following Table 6 and Figures 5, 6 and 7.

In Table 6, in which, for $636 \leq V_{oc}(mV) \leq 745$, the physical conditions used are those given in Eq. (50), according to the CTER, we will get the precisions of the order of 9.1% for J_{sc}, 6% for FF, and 9.8% for η, calculated using the corresponding data [2, 18, 19, 20, 25, 29, 30], being strongly affected by $J_o = J_{Eo} + J_{Bo}$, as noted above. One can conclude here that, with such high accuracies of these performance parameters, our obtained J_{Eo}-results given in Table 4, using Equations (40, 9), may be accurate within about 9.8%.

Table 6. With the physical conditions given in Eq. (58), our present results (PR) of n, J_{sc}, FF, and η, calculated using Equations (52, 51, 56, 57), being compared with corresponding data (D), and their relative deviations (RD), computed using the formula: RD=$|1-(PR/D)|$. VC

Data (D) from References	V_{oc} (mV)	n	$J_{sc(PR)}(J_{sc(D)})$;RD $(\frac{mA}{cm^2})$ $(\frac{mA}{cm^2})$ (%)	$FF_{(PR)}(FF_{(D)})$;RD (%) (%) (%)	$\eta_{(PR)}(\eta_{(D)})$;RD (%) (%) (%)
[2]	745	1.6968	40.66 (39.4); 3.2	79.79 (80.9); 1.4	24.17 (23.7); 1.9
[2]	729	1.6591	41.18 (38.5); 6.9	79.80 (79.1); 0.9	23.95 (22.1); 8.4
[2]	735	1.6732	41.00 (38.5); 6.5	79.80 (77.5); 3.0	24.05 (21.9); 9.8
[2]	726	1.6521	41.26 (37.8); 9.1	79.80 (79.7); 0.1	23.90 (21.8); 9.6
[2]	639	1.4619	37.70 (39.3); 4.1	79.73 (78.9); 1.0	19.20 (19.8); 3.0
[25]	655	1.4934	39.90 (39.5); 1.0	79.77 (79.9); 0.1	20.85 (20.7); 0.7
[25]	656	1.4955	39.99 (39.5); 1.2	79.80 (79.8); 0.0	20.93 (20.7); 1.1
[20]	727	1.6544	41.23 (38.9); 6.0	79.80 (78.4); 1.8	23.92 (22.1); 8.0
[29]	704	1.6012	41.60 (41.6); 0.0	79.81 (83.5); 4.4	23.37 (24.5); 4.6
[29]	704	1.6012	41.60 (41.5); 0.2	79.81 (81.0); 1.5	23.37 (23.7); 1.4
[29]	712	1.6196	41.53 (38.4); 8.1	79.81 (78.7); 1.4	23.60 (21.5); 9.7
[29]	678	1.5428	41.27 (39.5); 4.5	79.80 (80.3); 0.6	22.33 (21.5); 3.9
[29]	636	1.4568	36.90 (36.9); 0.0	79.71 (77.0); 3.5	18.71 (18.1); 3.3
[18]	677	1.5406	41.24 (40.3); 2.3	79.80 (80.6); 0.9	22.28 (22.0); 1.3
[18]	729	1.6591	41.18 (39.6); 3.9	79.80 (80.0); 0.2	23.95 (23.0); 4.1
[18]	704	1.6012	41.60 (41.9); 0.7	79.80 (81.0); 1.5	23.37 (23.9); 2.2
[19]	651	1.4852	39.49 (38.8); 1.8	79.76 (76.4); 4.4	20.51 (19.3); 6.2
[19]	721	1.6404	41.37 (40.5); 2.1	79.80 (82.9); 3.7	23.80 (24.2); 1.6
[19]	704	1.6012	41.60 (42.0); 0.9	79.81 (83.5); 4.4	23.37 (24.7); 5.4
[30]	738	1.6802	40.91 (42.6); 4.1	79.79 (84.9); 6.0	24.09 (26.7); 9.7
[30]	674.2	1.5345	41.13 (41.1); 0.1	79.80 (80.5); 0.9	22.13 (22.3); 0.8
[30]	687	1.5628	41.50 (38.5); 7.8	79.81 (80.3); 0.6	22.75 (21.2); 7.3

The underlined RD(%)-values are the maximal ones, being equal to: 9.1% at $V_{oc} = 726$ mV for $J_{sc(PR)}$, 6.0% at $V_{oc} = 738$ mV for $FF_{(PR)}$, and 9.8% at $V_{oc} = 735$ mV for $\eta_{(PR)}$.

In Figures 5 (a), (b), (c) and (d), the physical conditions used are:

$$N = 10^{20}\ cm^{-3}, r_a = r_B, N_d = 10^{16}\ cm^{-3}, r_d = r_P, \text{and different } (S, W) - \text{values.} \quad (53)$$

Here, for a given V_{oc}, and with decreasing S and increasing W, we observe that:

(i) in the Fig. 5 (a), the function n (or the function J_o given in Table 5) decreases from the CTER to the COER,

(ii) in Figures 5 (b), 5 (c) and 5(d), the functions J_{sc}, FF and η therefore increase from the CTER to the COER, and

(iii) in Figure 5 (d), for the physical functions: W=136 μm and $S = 10^{-50}$ cm/s, the function η reaches a maximum equal to 27.36% at V_{oc}=742 mV; here $1\ \mu m = 10^{-6}$ m.

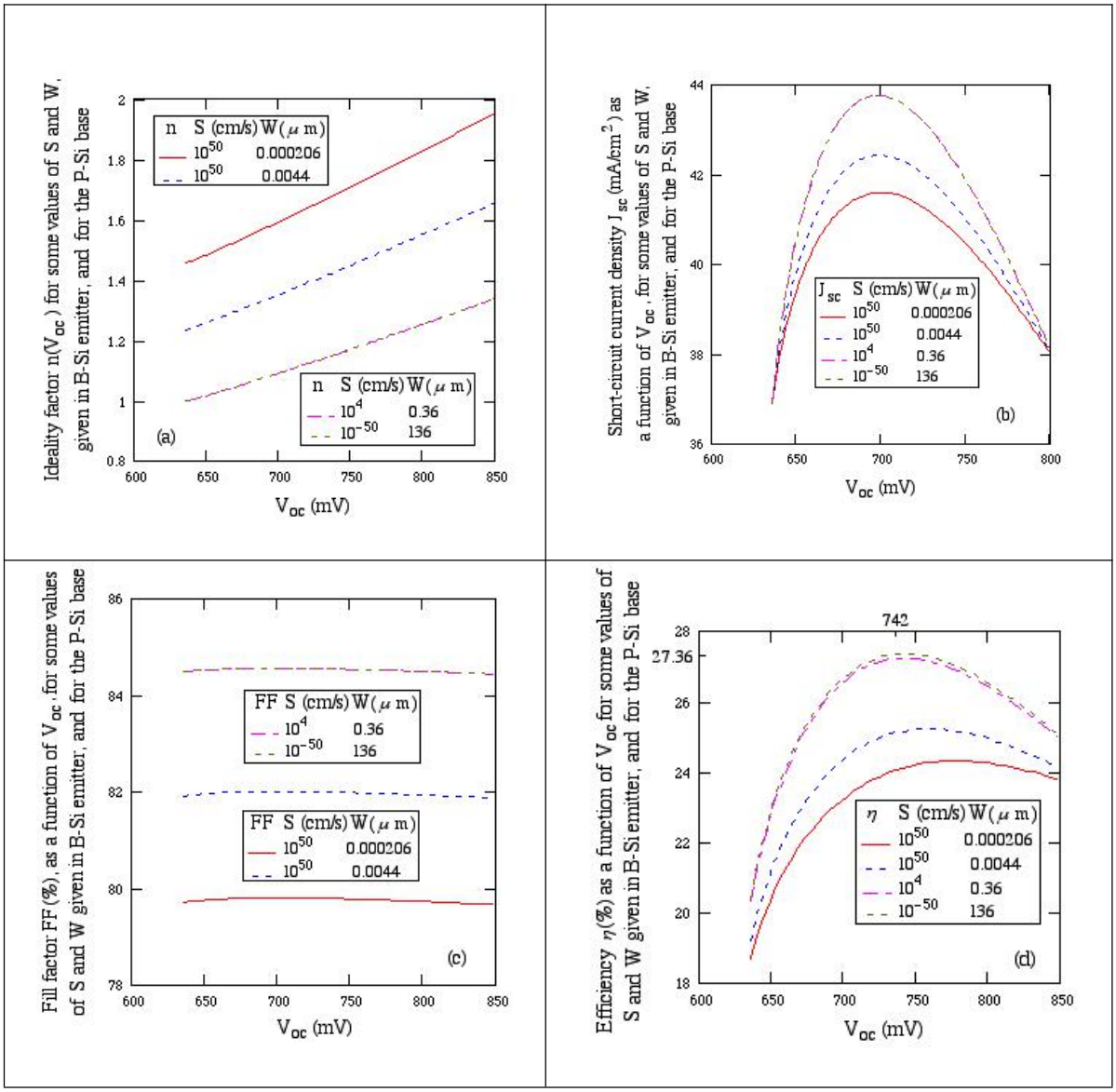

Figure 5. (a) Our n-results, (b) $J_{sc}(\frac{mA}{cm^2})$-results, (c) FF(%)-results, and (d) η(%)-results, plotted as functions of V_{oc} and obtained with increasing W and decreasing S (or from the completely transparent emitter region to the completely opaque emitter region).

In Figures 6 (a), (b), (c) and (d), the physical conditions used are:

$$W = 136\ \mu m,\ N = 5 \times 10^{20}\ cm^{-3}, r_a = r_{Tl},\ S = 10^{-50}\frac{cm}{s},$$
$$N_d = 10^{16}\ cm^{-3},\ r_d, \text{ and } E_{gi}(r_d) \text{ at } 300\ K, \tag{54}$$

according to the COER, and they are also given in these Figures and in Table 5 for the second limiting case, in which $J_o = J_{Bo}$, since $J_{Eo} = 0$. Thus, this simplifies the numerical calculation of functions n, J_{sc}, FF and η, using Equations (48, 47, 51, 52), where J_o is replaced by J_{Bo}, determined by Eq. (17). Further, in Equation (54), the values of $E_{gi}(r_d)$ are given in Table 2. Then, for a given V_{oc} and with increasing r_d-values, it should be concluded that, due to the acceptor-size effect,

(i) in the Fig. 6 (a), the function n (or the function J_o given in Table 5) decreases (↓), and

(ii) in Figures 6 (b), (c), (d), the functions J_{sc}, FF and η therefore increase (↑), and in particular, in Fig. 6 (d), for the completely opaque (Tl-Si) emitter-region conditions, where J_{Eo}=0 or $J_o = J_{Bo}$, the maximal η-values are equal to: 27.35 %,…, 27.56 %, at V_{oc}=742 mV,…,739 mV, according to the E_{gi}-values equal to: 1.11 eV,…, 1.70 eV, which are obtained in various lightly doped (Sb,…, S)-Si base regions, respectively, being due to the donor-size effect.

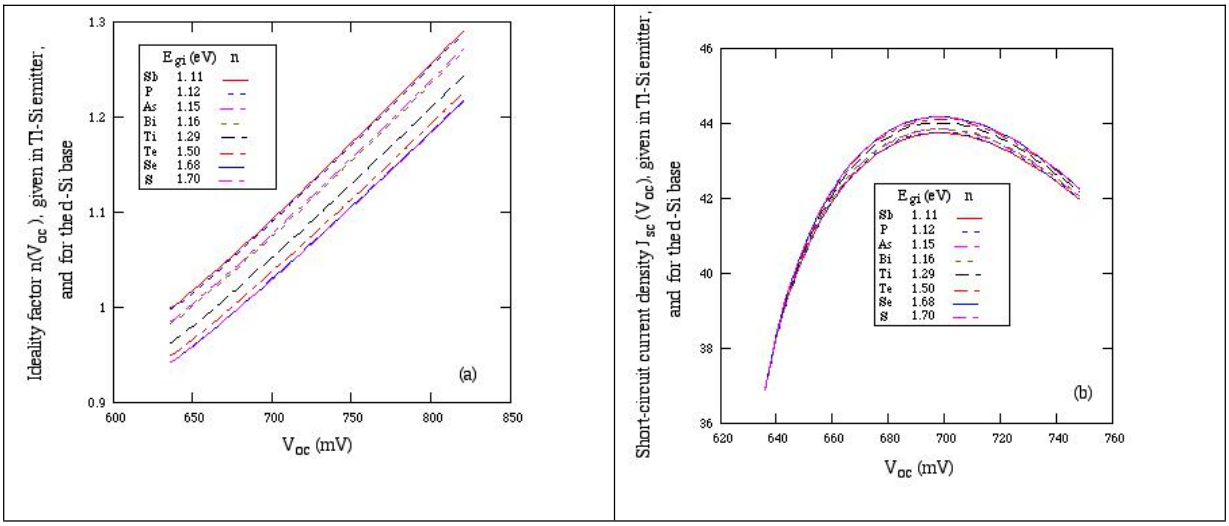

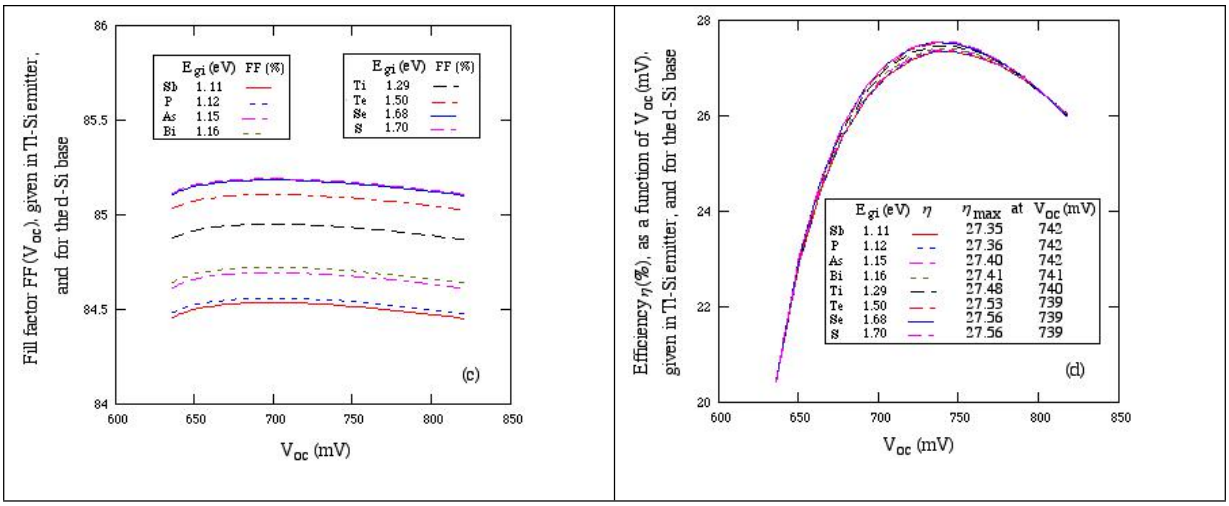

Fig. 6. (a) Our n-results, (b) $J_{sc}(\frac{mA}{cm^2})$-results, (c) FF(%)-results, and (d) η(%)- results, plotted as functions of V_{oc}, and obtained in the COER-conditions, as those given in Eq. (54).

Finally, in Figures 7 (a), (b), (c) and (d), the physical conditions used are:

$$W = 0.000206\ \mu m,\ N = 5 \times 10^{20}\ cm^{-3},\ r_a,\ S = 10^{50}\frac{cm}{s},$$

$$N_d = 10^{16}\ cm^{-3},\ r_d = r_S,\ \text{and}\ E_{gi}(r_a)\ \text{at}\ 300\ K, \tag{55}$$

according to the CTER, and they are also given in Table 5 for the third case. Here, the values of $E_{gi}(r_a)$ at 300 K are given in Table 2. Then, the numerical results of n, J_{sc}, FF and η are calculated, using Equations (48, 47, 51, 52). Further, for a given V_{oc} and with increasing r_a-values, it should be concluded that, due to the acceptor-size effect,

(i) in the Fig. 7 (a), the function n determined in Equation (52) (or the function J_o given in Table 5) decreases (↓), and

in Figures 7 (b), (c), (d), the functions J_{sc}, FF and η therefore increase (↑), and in particular, in Fig. 7 (d), in the conditions of completely transparent and heavily doped (acceptor-Si) emitter-and- lightly doped (S-Si) base regions, the maximal η-values are equal to: 24.59 %,…, 26.52 %, at V_{oc}=771 mV,…,743 mV, according to the E_{gi}-values equal to: 1.1245 eV,…, 1.3415 eV, obtained in various (B,…, Tl)-Si emitter regions, respectively, being due to the acceptor-size effect.

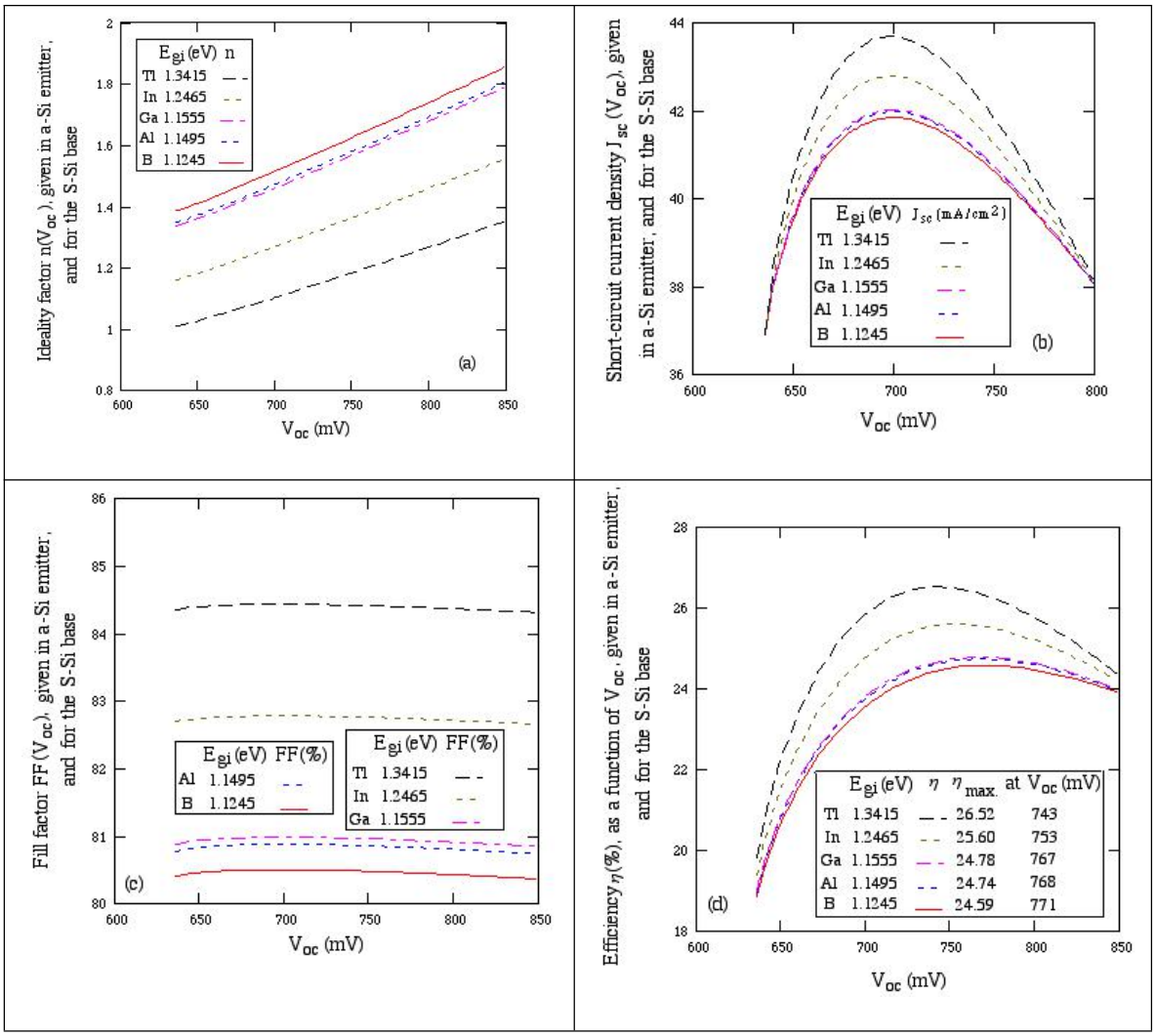

Fig. 7. (a) Our n-results, (b) $J_{sc}(\frac{mA}{cm^2})$-ones, (c) FF(%)-ones, and (d) η(%)-ones, plotted as functions of V_{oc} and obtained in the CTER-conditions.

7. Concluding Remarks

We have developed the effects of heavy doping and impurity size on various parameters at 300 K, characteristic of energy-band structure, as given in Sections 2 and 3, and of the performance of crystalline silicon emitter (base) regions of $p^+ - n$ junction solar cells, being strongly affected by the dark saturation current density: $J_o \equiv J_{Eo} + J_{Bo}$, as given in Sections 4, 5 and 6. Then, some concluding remarks are obtained and discussed as follows.

(i) Using the optical band gap (E_{g1})-data given by Wagner and del Alamo [45], our E_{g1}-results, due to the heavy doping effect and calculated using Eq. (12), are found to be accurate within 1.88%, as observed in Table 3.

(ii) In the CTER-conditions, as those given in Table 4, and using the J_{Eo}-data, given by Cuevas et al. [22], and Equations (40, 9) and Equations (40, 11), our J_{Eo}-results, obtained in

the heavily doped and completely transparent (B-Si) emitter region, are found to be accurate within 32.9% and 19.4%, respectively, while the calculated J_{Eo}-results, obtained by Cuevas et al. [22], are accurate within 220%.

(iii) For given physical conditions and using an empirical treatment method of two points, as developed and discussed in Section 6, both our two results (n and J_o) have the same variations, which strongly affect other (V_{oc}, J_{sc}, FF, η)-results, as discussed in Eq. (49), indicating that J_o, determined in Eq. (43), is a central result of our present paper.

(iv) In the CTER-conditions, as those given in Eq. (50), and using various (J_{sc}, FF, η)-data [2, 18, 19, 20, 25, 29, 30], we get the precisions of the order of 9.1% for J_{sc}, 6% for FF and 9.8% for η, being strongly affected by $J_o = J_{Eo} + J_{Bo}$, as noted above. Thus, we can conclude here that, with such high accuracies of these performance parameters, our obtained J_{Eo}-results given in Table 4, using Equations (40, 9), may be accurate within about 9.8%.

(v) In the physical conditions of completely opaque and heavily doped (Tl-Si) emitter-and-lightly doped (donor-Si) base regions, as given in Eq. (54), and in the physical conditions of completely transparent and heavily doped (acceptor-Si) emitter-and-lightly doped (Tl-Si) base regions, as given in Eq. (55), our calculated maximal η-values, due to the impurity-size effect, are found to be equal to: 27.35%, …, 27.56%, as seen in Figure 6 (d), and 24.59%, …, 26.52%, as observed in Figure 7 (d), respectively. So, the highest η-value, obtained in the present paper is equal to: $\eta(\text{present}) = 27.56\%$, obtained in the condition of completely opaque and heavily doped (Tl-Si) emitter-and-lightly doped (S-Si) base regions, with $E_{gi}(r_{Tl}) = 1.34$ eV, while in our previous paper [1] we got: $\eta(\text{previous}) = 31.55\%$, obtained in the condition of completely opaque and heavily doped (S-Si) emitter-and-lightly doped (Tl-Si) base regions, with $E_{gi}(r_S) = 1.70$ eV $> E_{gi}(r_{Tl}) = 1.34$ eV, being due to the impurity-size effect, because of $r_S > r_{Tl}$, as seen in Table 1. Furthermore, those results can be compared with a well-known highest η-value, obtained by Richter et al. (R) [27], $\eta(R) = 29.43\%$, as: $\eta(\text{present}) = 27.56\% < \eta(R) = 29.43\% < \eta(\text{previous}) = 31.55\%$.

Acknowledgments: We thank Prof. Dr. Nghi Q. Lam, the Former Editor-in-Chief of Applied Physics Letters (1994-2014), for his helpful remarks and suggestions, which have greatly improved the presentation of our paper.

References

[1] H. Van Cong, P. Blaise, and O. Henri-Rousseau, "Effects of heavy doping and impurity size on minority-carrier transport parameters in heavily (lightly) doped n(p)-type crystalline silicon at 300 K, applied to determine the performance of $n^+ - p$ junction solar cells," to be published in SCIREA Journal of Physics.

[2] S. De Wolf, A. Descoeudres, Z. C. Holman, and C. Ballif, "High-efficiency silicon heterojunction solar cells: a review," Green, vol. 2, pp. 7-24, 2012.

[3] W. Shockley, "The theory of p-n junctions in semiconductors and p-n junction transistors," Bell Syst. Tech. J., vol. 28, pp. 435-489, 1949; W. Shockley and H. J. Queisser, " Detailed balance limit of efficiency of p-n junction solar cells." J. Appl. Phys., vol. 32, pp. 510-519, 1961.

[4] J. W. Slotboom, H. C. de Graaff, "Measurements of band gap narrowing in Si bipolar transistors," Solid-State Electron., vol. 19, pp. 857-862, 1976.

[5] M. A. Green, "Solar cell fill factors: general graph and empirical expressions," Solid-State Electron., vol. 24, pp. 788-789, 1981; M. Leilaeioun and Z. C. Holman,"Accuracy of expressions for the fill factor of a solar cell in terms of open-circuit voltage and ideality factor," *J. Appl. Phys.*, vol. 120, pp. 123111, 2016.

[6] R. M. Swanson and R. A. Sinton," Advances in Solar Energy," edited by K. A. Bouer , American Solar Energy, Newark, Delaware, 1990.

[7] H. P. D. Lanyon, "The Physics of heavily doped $n^+ - p$ junction solar cells," Solar Cells," vol. 3, pp. 289-311, 1981; H. Van Cong and S. Brunet, "Effective drift current densities in the n-type heavily doped emitter region of $p - n^+$ junction silicon solar cells, "Solar Cells," vol. 5, pp. 355-365, 1982; H. Van Cong and S. Brunet, S. Charar, J. L. Birman, and M. Averous, "Optical and electrical energy gaps of the n-type impure silicon at 300 K," Solid State Commun., vol. 45, pp. 611-614, 1983.

[8] M. A. Shibib, F. A. Lindholm, and F. Therez, "Heavily doped transparent-emitter region in junction solar cells, diodes, and transistors," IEEE Trans. Electron Devices, vol. ED-26, pp.959-965, 1979; M. A. Shibib and J. G. Fossum, "Limitations on the open-circuit voltage imposed by p^+ and n^+ regions in silicon solar cells," J. Appl. Phys., vol. 52, pp. 1072-1075, 1981.

[9] J. del Alamo and R. M. Swanson, "The physics and modeling of heavily doped emitters," IEEE Trans. Electron Devices, vol. ED-31, pp. 1878-1888, 1984; J. del Alamo, S. Swirhum, and R. M. Swanson,"Measurement of steady-state minority-carrier transport

parameters in heavily doped n-type silicon," IEEE Trans. Electron Devices, vol. ED-34, pp. 1580-1589, 1987.

[10] R. A. Logan, J. F. Gilbert, and F. A. Trumbore, "Electron mobilities and tunneling currents in silicon, "J. Appl. Phys.," vol. 32, pp. 131-132, 1961.

[11] J. del Alamo, S. Swirhum, and R. M. Swanson, "Measuring and modeling minority carrier transport in heavily doped silicon, "Solid-State Electron.," vol. 28, pp. 47-54, 1985; J. del Alamo, S. Swirhum, and Swanson R. M., "Simultaneous measurement of hole lifetime, hole mobility, and band gap narrowing in heavily doped n-type silicon," Int. Electron Devices Meet. Tech. Dig.," vol. 31, pp. 290-293, 1985.

[12] D. Chattopadhyay and H. J. Queisser, "Electron scattering by ionized impurities in semiconductors," Rev. Mod. Phys., vol. 53, pp. 745-768, 1981.

[13] R. M. Swanson, "Modeling of minority-carrier transport in heavily doped silicon emitters, "Solid-State Electron.," vol. 30, pp. 1127-1136, 1987.

[14] Z. Essa, N. Taleb, B. Sermage, C. Broussillon, B. Bazer-Bachi, and M. Quillec, "Doping profile measurement on textured silicon surface," EPJ Photovoltaics, vol. 9, p. 5, 2018.

[15] S. C. Jain, E. L. Heasell, and D. J. Roulston, "Recent advances in the physics of silicon p-n junction solar cells including their transient response," Prog. Quant. Electron., vol. 11, pp. 105-204, 1987.

[16] S. C. Jain and D. J. Roulston, "A simple expression for band gap narrowing in heavily doped Si, Ge, GaAs and Ge_xSi_{1-x} strained layers," Solid-State Electron., vol. 34, pp. 453-465, 1991.

[17] D. B. M. Klaassen, J. W. Slotboom, and H. C. de Graaff, "Unified apparent band gap narrowing in n- and p-type silicon," Solid-State Electron., vol. 35, pp. 125-129, 1992; D. B. M. Klaassen, "A unified mobility model for device simulation-II, "Temperature dependence of carrier mobility and lifetime," Solid-State Electron., vol. 35, pp. 961-967, 1992.

[18] M. A. Green, K. Emery, Y. Hisikawa, and W. Warta, "Solar cell efficiency Tables (Version 36)," Prog. Photovolt: Res. Appli., vol. 18, pp. 346-352, 2010.

[19] M. A. Green, K. Emery, Y. Hisikawa, and W. Warta, "Solar cell efficiency Tables (Version 37)," Prog. Photovolt: Res. Appli., vol. 19, pp. 84-92, 2011.

[20] A. Descoeudres, Z. C. Holman, L. Barraud, S. Morel, S. De Wolf, and C. Ballif, "21% efficiency silicon heterojunction solar cells on n- and p- type wafers compared," IEEE Journal of Photovoltaics, vol. 3, pp. 83-89, 2013.

[21] F. H. Alharbi and S. Kais, “Theoretical limits of photovoltaics efficiency and possible improvements by intuitive approaches learned from photosynthesis and quantum coherence, ”Renewable and sustainable energy reviews,” vol. 43, pp. 1073-1089, 2015.

[22] A. Cuevas, J. G. Fossum, and R. T. Young, “Influence of the dopant density profile on minority-carrier current in shallow, heavily doped emitters of silicon bipolar devices,” Solid-State Electron., vol. 28, pp. 247-254, 1985.

[23] H. Van Cong, “A simple accurate solution to minority electron injection in the p-type heavily doped emitter region of silicon devices,” Physica Status Solidi A, Vol. 149, pp. 619-628, 1995; H. Van Cong and G. Debiais, “About a conjunction between electrical and optical phenomena in p-type heavily doped silicon at room temperature,” Physica Status Solidi B, vol. 191, pp. 161-169, 1995.

[24] M. A. Green, K. Emery, Y. Hisikawa, W. Warta, E. D. Dunlop, D. H. Levi, and A. W. Y. Ho-Baillie, “Solar cell efficiency Tables (Version 49),” Prog. Photovolt: Res. Appli., vol. 19, pp. 84-92, 2011.

[25] A. Fell, K. R. McIntosh, P. P. Altermatt, G. J. M. Janssen, R. Stangl, A. Ho-Baillie, H. Steinkemper, J. Greulich, M. Müller, B. Min, K. C. Fong, M. Hermle, I. G. Romijn, and M. D. Abbott, “Input Parameters for the simulation of silicon solar cells in 2014,” IEEE J. Photovoltaics, vol. 5, pp. 1250-1263, 2015.

[26] H. Van Cong and G. Debiais, “Energy band structure parameters and their data, derived from the measurements of minority carrier current density in heavily doped emitters of silicon devices,” Solar Ener. Mater. and Solar Cells, vol. 45, pp. 385-399, 1997; H. Van Cong and G. Debiais, “Apparent band-gap narrowing and its data derived from the measurements of minority-carrier current density in heavily doped emitters of silicon devices,” Physica Status Solidi A, vol. 155, pp. 547-553, 1996; H. Van Cong, “A new solution for minority-carrier injection into the heavily doped emitter of silicon devices,” Physica Status Solidi A, vol. 171, pp. 631-645, 1999.

[27] A. Richter, M. Hermle, and S. W. Glunz, “ Reassessment of the limiting efficiency for crystalline silicon solar cells,” IEEE J. Photovoltaics, vol. 3, pp. 1184-1191, 2013.

[28] R. S. Davidsen, H. Li, A. To, X. Wang, A. Han, J. An, J. Colwell, C. Chan, A. Wenham, M. S. Schmidt, A. Boisen, O. Hansen, S. Wenham, and A. Barnett, “Black silicon laser-doped selective emitter solar cell with 18.1% efficiency,” Sol. Energy Mater. Sol. Cells,” vol. 144, pp. 740-747, 2016.

[29] M. A. Green, K. Emery, D. L. King, Y. Hisikawa, and W. Warta, “Solar cell efficiency Tables (Version 27),” Prog. Photovolt: Res. Appli., vol. 14, pp. 45-51, 2006.

[30] M. A. Green, Y. Hishikawa, E. D. Dunlop, D. H. Levi, J. Hohl-Ebinger, and A. W. Y. Ho-Baillie, "Solar cell efficiency tables (version 51)," Prog. Photovolt. Res. Appl., vol. 26, pp. 3-12, 2018.

[31] J. E. Lang, F. L. Madarasz, and P. M. Hemenger, "Temperature dependent density of states effective mass in non-parabolic p-type silicon," J. Appl. Phys., vol. 54, pp. 3612-3612, 1983.

[32] M. A. Green, "Intrinsic concentration, effective densities of states, and effective mass in silicon," J. Appl. Phys., vol. 67, pp. 2944-2954, 1990.

[33] H. Van Cong, "Band gap changes in excited intrinsic (heavily doped) Si and Ge semiconductors," Physica B, vol. 405, pp. 1139-1149, 2010.

[34] R. Pässler, "Dispersion-related description of temperature dependencies of band gaps in semiconductors," Phys. Rev. B, vol. 66, p. 085201, 2002.

[35] R. Pässler, "Semi-empirical descriptions of temperature dependences of band gaps in semiconductors," Physica Status Solidi B, vol. 236, pp. 710-728, 2003.

[36] O. Henri-Rousseau and P. Blaise, Quantum Oscillators, edited by John Wiley & Sons, Inc., Hoboken, New Jersey, 2011; O. Henri-Rousseau, Physique Théorique et Réalité, edited by Collection Etudes, Presses Universitaires de Perpignan, 2018.

[37] A. B. Sproul and M. A. Green, "Improved value for the silicon intrinsic carrier concentration from 275 to 375 K," J. Appl. Phys., vol. 70, pp. 846-854, 1991; A. B. Sproul and M. A. Green, "Intrinsic carrier concentration and minority-carrier mobility of silicon from 77 to 300 K," J. Appl. Phys., vol. 73, pp. 1214-1225, 1993.

[38] K. Misiakos and D. Tsamakis, "Accurate measurements of the silicon intrinsic carrier density from 77 to 340 K," J. Appl. Phys., vol. 74, pp. 3293-3297, 1993.

[39] R. Couderc, M. Amara, and M. Lemiti, "Reassessment of the intrinsic carrier density temperature dependence in crystalline silicon," J. Appl. Phys., vol. 115, p. 093705, 2014.

[40] H. Van Cong and G. Debiais, "A simple accurate expression of the reduced Fermi energy for any reduced carrier density," J. Appl. Phys., vol. 73, pp. 1545-15463, 1993.

[41] H. Van Cong and B. Doan Khanh, "Simple accurate general expression of the Fermi-Dirac integral $F_j(a)$ for arbitrary a and j> -1," Solid-State Electron., vol. 35, pp. 949-951, 1992; H. Van Cong, "New series representation of Fermi-Dirac integral $F_j(-\infty < a < \infty)$ for arbitrary j> -1, and its effect on $F_j(a \geq 0_+)$ for integer $j \geq 0$," Solid-State Electron., vol. 34, pp. 489-492, 1991.

[42] H. Van Cong, S. Abide, B. Zeghmati, and X. Chesneau, “Optical band gap in various impurity-Si systems from the metal-insulator transition study,” Physica B, vol. 436, pp. 130-139, 2014.

[43] H. Van Cong, “Effects of impurity size and heavy doping on energy-band-structure parameters of various impurity-Si systems,” Physica B, vol. 487, pp. 90-101, 2016.

[44] H. Van Cong, “Effects of donor size and heavy doping on optical, electrical and thermoelectric properties of various degenerate donor-silicon systems at low temperatures,” American Journal of Modern Physics, vol. 7, pp. 136-165, 2018; H. Van Cong, S. Brunet, and J. C. Martin, “Size effect on different impurity levels in semiconductors,” Solid State Commun., vol. 49, pp. 697-699, 1984.

[45] J. Wagner and J. A. del Alamo, “Band-gap narrowing in heavily doped silicon: A comparison of optical and electrical data,” J. Appl. Phys., vol. 63, pp. 425-429, 1988.

[46] H. Van Cong, “Fermi energy and band-tail parameters in heavily doped semiconductors,” J. Phys. Chem. Solids, vol. 36, pp. 1237-1240, 1975.